Applied Energy 222 (2018) 951–966

Contents lists available at ScienceDirect

Applied Energy

journal homepage: www.elsevier.com/locate/apenergy

An MILP framework for optimizing demand response operation of air separation units

Morgan T. Kelley[a], Richard C. Pattison[a,1], Ross Baldick[b], Michael Baldea[a,*]

[a] McKetta Department of Chemical Engineering, The University of Texas at Austin, Austin, TX 78712, United States
[b] Department of Electrical and Computer Engineering, The University of Texas at Austin, Austin, TX 78712, United States

HIGHLIGHTS

- Focus on demand response (DR) scheduling of air separation units (ASUs), a class of electricity-intensive chemical plants.
- Provide a novel scheduling framework that accounts for plant dynamics.
- Dynamic models are identified from historical operating data.
- A Lagrangian relaxation scheme is developed, providing excellent computational results.
- Extensive simulation studies show considerable reductions in operating cost and peak power demand.

ARTICLE INFO

Keywords:
Demand response
Air separation
Production scheduling
Lagrangian relaxation

ABSTRACT

Peaks in renewable electricity generation and consumer demand are desynchronized in time, posing a challenge for grid operators. Industrial demand response (DR) has emerged as a candidate for mitigating this variability. In this paper, we demonstrate the application of DR to an air separation unit (ASU). We develop a novel optimal production scheduling framework that accounts for day-ahead electricity prices to modulate the grid load presented by the plant. We account for the dynamics of the plant using a novel dynamic modeling strategy, which allows us to formulate the corresponding optimization problem as a mixed integer linear program (MILP). Further, we present a new relaxation scheme that affords fast solutions of this MILP. Extensive simulation results show significant reductions in operating costs (that benefit the plant) and reductions in peak power demand (that benefit the grid).

1. Introduction

The structure of the electricity industry has changed in recent years. Increases in demand due to population growth, changes in supply mix/location, increasing variability due to renewable integration, and increasing threats to reliability and security due to weather and other events created a need to modernize the electricity grid [1]. Such challenges have led to the advent of the smart grid, whose goals include reducing the frequency and duration of power outages through the use of new technologies, equipment, and control strategies [1].

Demand Response (DR) has become an important resource for modernizing the electricity grid. DR involves reducing electricity usage during peak demand times, thereby lessening stress on the grid. Key drivers for DR involvement include the introduction of time-based electricity rates such as time-of-use, variable peak, and real-time pricing. Industrial, residential, and commercial customers can all participate in DR. While all three classes of users are suitable for DR, industrial users will be the focus of this work. Industrial customers typically have large electricity loads and therefore are true "needle movers," contributing the largest percentage (32%) of the total yearly electricity consumption per year in the US [2]. In particular, the Chemical and Petroleum refining industries combined accounted for 58% of the total industrial electricity usage in the US in 2013 [3].

Furthermore, industrial users are particularly well-suited for engaging in DR programs, given the lack of human-centered daily time-based demand fluctuations, such as the use of air conditioning and heating. Under DR operation, an industrial site would typically increase production during off-peak hours, storing product in excess of demand and later use this product to meet demand during peak grid load times, when production rates are lowered to reduce power consumption. Such

* Corresponding author.
E-mail address: mbaldea@che.utexas.edu (M. Baldea).
[1] Richard C. Pattison is currently with Apeel Sciences, Goleta, CA 93117, United States.

https://doi.org/10.1016/j.apenergy.2017.12.127
Received 6 October 2017; Received in revised form 12 December 2017; Accepted 30 December 2017
Available online 09 May 2018
0306-2619/ © 2017 Elsevier Ltd. All rights reserved.

Symbol & definition

Sets

i	scheduling time slot
j	dynamics time intervals
k	piecewise linear breakpoints
m	Lagrangian relaxation iteration
n	distillation column stage

Continuous variables

t	time
u_i	scale-bridging model input (production set-point)
h_i	Hammerstein block output
$\overrightarrow{x}_{i,j}$	state variable
$\overrightarrow{y}_{i,j}$	state-space output
$w_{i,j}$	scale-bridging model output
$\overrightarrow{w}_{i,j}$	vector of scheduling-relevant variables
$\overrightarrow{w}^{s}_{i,j}$	vector of storage-relevant variables
$\lambda^{H}_{i,k}$	special ordered sets of type 2 variable for Hammerstein block
$\lambda^{W}_{i,j,k}$	special ordered sets of type 2 variable for Wiener block
$s_{i,j}$	storage holdup (mol)
$f^{in/out}_{s_{i,j}}$	flowrate into/out of storage (mol/s)
$\gamma_{i,m}$	complicating constraint violation
$F^{p}_{i,j}$	production rate (mol/s)
$I^{p}_{i,j}$	impurity level in product stream (ppm)
$F^{f}_{i,j}$	feed flowrate (mol/s)
$M^{r}_{i,j}$	reboiler holdup (kmol)
$\delta^{f}_{n,i,j}$	column flooding fraction
$v_{n,i,j}$	vapor velocity at tray n
$v^{flood}_{n,i,j}$	flooding velocity at tray n
$P^{d}_{i,j}$	dew-point pressure ratio
$P^{zone1}_{i,j}$	heat exchanger zone 1 pressure
$P^{dew}_{i,j}$	dew point pressure
$P^{b}_{i,j}$	bubble-point pressure ratio
$P^{zone2}_{i,j}$	heat exchanger zone 2 pressure
$P^{bub}_{i,j}$	bubble point pressure
$\Delta T_{i,j}$	minimum temperature difference accross the reboiler/condenser (°C)
$T^{cond}_{i,j}$	condenser temperature (°C)
$T^{reb}_{i,j}$	reboiler temperature (°C)
$\mathscr{P}_{i,j}$	power requirements for the entire plant (MW)
$\mathscr{W}_{i,j}$	net work of compressors, turnbines, and liquefier

Binary variables

$z^{H}_{i,k}$	binary variable for input (Hammerstein) SOS2 linearization
$z^{W}_{i,j,k}$	binary variable for output (Wiener) SOS2 linearization

Parameters and coefficients

N_I	number of scheduling time slots
T_I	length of scheduling time slot i
N_J	number of points for discretizing dynamics
T_J	length of each dynamics time slot j
τ_{dom}	dominant system time constant
α	timescale conversion factor
D	demand (mol/s)
$Price_i$	associated (time-based) electricity price
$pw^{H}_{i,k}$	value of the Hammerstein piecewise linear function at breakpoint k
$bp^{H}_{i,k}$	breakpoint k of piecewise linear Hammerstein function
$pw^{W}_{i,j,k}$	value of the Wiener piecewise linear function at breakpoint k
$bp^{W}_{i,j,k}$	breakpoint k of piecewise linear Wiener function
Θ	Lagrangian Relaxation (LR) termination tolerance
$LD_{i,m}$	Lagrange multiplier
$\Gamma_{i,m}$	positive parameter for Lagrangian multiplier calculation
S_j	Finite Step Response (FSR) model parameter
Ω	parameter for net work calculation
$Stepsize_{i,m}$	stepsize for Lagrangian relaxation
ϵ	small parameter for Lagrangian relaxation

a scheme essentially relies on the storage of energy in the form of physical products. Thus, in order to participate in DR, an industrial site must not only be able to store products safely and efficiently, but also must be able to modulate its production rate related to electricity demand on the same timescale as the fluctuations of the load on the power grid, as reflected in electricity price changes.

Changes in electricity prices can occur at different frequencies, ranging from every several hours to, in some cases, every 5 min [4]. These changes are on the same time-scale as the dynamics of process variables, and therefore, it becomes necessary to embed dynamic process models into DR production scheduling calculations to ensure that scheduling moves account for the relevant dynamic behavior [5–7]. Embedding information on process dynamics and control in scheduling calculations is challenging: the relevant dynamic models are typically large-scale, nonlinear, and stiff, given the complicated nature of process dynamics and the multiple time-scales involved in making scheduling and control decisions.

We base this paper on a previous work [8] where we address these issues for the specific case of an Air Separation Unit (ASU) with variable production rate participating in DR. The ASU herein is assumed to be a participant in a market where hourly electricity prices are known (or can be accurately predicted) 72 h in advance, with the goal of optimizing the production schedule to minimize operating cost. In particular, we propose using (nonlinear) low-order data-driven models of the scheduling-relevant dynamics of the plant [8], and present a set of reformulation and (exact) linearization techniques that allow us to cast the overall DR scheduling problem as Mixed Integer Linear Program (MILP). We show that DR operation can lead to significant savings in operating costs compared to a scenario where the production rate is kept constant during the day. Additionally, the operation of the grid benefits from considerable reductions in the power demand presented by the plant during peak times. Furthermore, we demonstrate the computational efficiency of this MILP framework and its potential for real-time implementation.

While the developments presented in the paper are centered on the operation of an ASU as a prototype large-scale electricity consumer (in effect, electricity represents *the only* paid feedstock of an ASU, since air is freely available), the framework we present here is general. Applying this strategy to all amenable industries (e.g., ammonia, chlor alkali [9–11]) could provide grid operators with considerable "breathing room" for incorporating more renewable resources while at the same time reducing the use of hydrocarbon-based power plants, thereby "decarbonizing" the power generation mix.

The paper is organized as follows: first, a review of previous studies focused on the modeling and operation of ASUs and current methods of embedding dynamics in scheduling calculations is provided. Then, the scheduling problem at hand is introduced, along with a review of the previously-developed model structures used to represent the ASU dynamics. A novel linear reformulation of these models is presented. The optimal scheduling problem and associated solution strategies are

discussed, followed by results in terms of the effect on both the power grid and the industrial site.

2. Literature review

Cryogenic distillation is the preferred method of air separation when high purity and high production rates are needed [12]. The purified components of air are used as feedstocks for many applications. For example, oxygen is used for steel production and for the production of various chemicals such as ethylene oxide in addition to frequent use in the medical field [13, p. 57–58]. Nitrogen is often used as an inert replacement for air in the food and pharmaceutical industries [13].

Air separation units typically use electricity to drive compressors that compress the feed air stream. These compressors have high electricity consumption; the industrial gas sector used 19.4 TW h of electricity in 2010 (2.5% of the total amount consumed by the manufacturing sector) in the US [14]. A significant amount of research has been completed with the goal of minimizing this energy usage via increasing unit operation efficiency [15] through process integration [16,17].

Further publications have discussed the potential advantages that stem from operating ASUs at a variable production rate, and have predicted significant cost savings in the presence of time-sensitive power prices (i.e., DR operation). A conceptual study published by Miller et al. [18] considered hourly electricity price variations for ASU operation. The profitability boundaries of a unit changing production rates in response to price fluctuations was defined using a maximum-to-minimum energy price ratio; values between 2 and 7 were deemed sufficient to motivate modulating the operation of a plant. This ratio estimate was, however, based on a simplified static plant model with an ideal work assumption for calculating the minimum ASU power requirement [18]. Other analyses relied on more detailed models. For example, Pattison et al. [19] developed a design blueprint for variable-capacity ASUs, showing that the design of the multi-stream heat exchanger may limit the agility of the process. A similar conclusion was reached by Cao et al. [20], who analyzed the process design aspects that can improve responsiveness of ASUs in DR scenarios. Zhang et al. [21] investigated the benefits of adding cryogenic energy storage (CES) to air separation plants considering demand uncertainty. The value of capital expenditures in increasing cryogenic air separation plant flexibility was also studied by Zhang et al. [22].

From an operations perspective, Ierapetritou et al. [23] and Karwan and Keblis [24] considered the optimal scheduling of ASUs with variable production rates and liquid storage tanks; these studies both relied on steady state linear models to represent process performance. Mitra et al. [25] considered transition behavior and its effect on modulating production rates using linear plant models. Zhu et al. [26] investigated the operation of an ASU subject to uncertainties arising from time-varying electricity prices and demand throughout the day with a multi-period formulation. This study used a detailed steady state nonlinear model, with approximated transition times to represent dynamics. However, the above approaches involving estimated transition times assume that the process reaches steady state between setpoint transitions. As previously mentioned, the process time constants are often comparable to the frequency of electricity price updates, and it is therefore unlikely that steady state is reached during production rate transitions in such a fast-changing market. Thus, such an assumption may lead to dynamically-infeasible operating schedules. In order to address this challenge, several works considered imposing rate-of-change constraints on changes in operating state [25,27]. In this way, scheduling calculations may circumvent the computational load associated with explicitly embedding dynamics. However, solutions obtained in this manner can lead to aggressive schedules which are dynamically infeasible [8]. Conversely, such constraints may produce overly conservative solutions [27] that are in fact not economically optimal. In a similar vein, Zhou et al. [28] utilized historical industrial data to describe operating modes on ASUs with load-change capabilities using convex hulls to determine the optimal schedule. In contrast, in our recent work we utilized low-order scale-bridging models (SBMs, which will be discussed in more detail below) to represent explicitly the nonlinear process dynamics in scheduling calculations in order to determine the optimal operating sequence for an ASU operating in fast-changing electricity markets [8]. We also note here the works of Cao et al. [29,30], which emphasize the importance of using dynamic models to study the operation of ASUs in the presence of fluctuations in demand and electricity prices, and seasonal changes in operating conditions.

The above studies indicate that the efficient integration of plant dynamics and control information in scheduling calculations for ASUs operating in fast-changing markets is an important consideration but remains a challenge. In this context, the main contributions of the present work are:

- a framework for defining data-driven reduced-order models, that are used to represent *nonlinear* ASU dynamics in DR scheduling calculations
- a model reformulation that allows us to re-cast the ASU DR scheduling problem as a mixed-integer *linear* program (MILP)
- a solution strategy that allows for short solution times and facilitates potential real-time implementation.

These developments are illustrated on an extensive case study representative of an industrial system. The results are compared and contrasted to current approaches for scheduling ASU operations, showing superior performance in terms of, (i) abiding by all the dynamic constraints posed by equipment limitations, product quality and process safety, while, (ii) providing for economic optimality in demand response operations.

3. Production scheduling for demand response

3.1. Background

In this work, we consider that the purpose of production scheduling for DR operation is to maximize profit (derived from operating under time-sensitive electricity prices), while, (i) meeting product demand and, (ii) abiding by all process constraints, related to e.g., product quality and safety. In this section, we discuss DR scheduling in the context of a process with a single product stream, whereby production can be continuously modulated within the confines of an upper and a lower bound, and product amounts exceeding demand can be stored and delivered to the customer at a later time. We place the DR scheduling problem within the broader context of the widely-accepted decision hierarchy followed in the operation of process systems (Fig. 1).

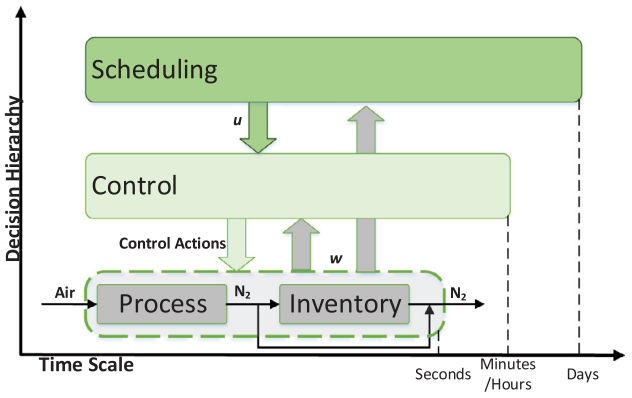

Fig. 1. Hierarchy of decisions made for process operation, where u are the production setpoints and w are the process variable levels.

The scheduling layer determines the optimal production sequence based on time-sensitive electricity prices. In this case, the production sequence is defined in terms of a (vector) of setpoint(s) concerning production rate and/or product quality, which are passed on to the control layer (as described below).

To provide more insight in the challenges faced by the scheduling layer, we present in Fig. 2 an example of day-ahead electricity prices, collected from the California Independent System Operator (CAISO) for an aggregate node in Fresno, CA. The data show that prices can fluctuate by a factor of five from the off-peak hours in the very early morning to the peak hours of the late afternoon of each day, with an additional smaller peak in the late morning. The data were collected during the month of October 2017 (which can be considered relatively "mild" from the point of view of ambient temperatures), and are thus representative of the "average" operation of the electricity market. We note that much more significant upswings are possible during very hot summer days, with demand (and price) increases mostly driven by residential consumers and the use of electricity-intensive air conditioners and household appliances.

The data set presented above shows hourly variations in electricity prices. For an industrial plant, and particularly a chemical process, capitalizing on these price changes would require that at the scheduling level the production rate targets be changed with hourly frequency as well. However, this time horizon is of the same magnitude (and, in effect, very likely shorter) than the time constant/settling time of the process. As consequence, the process is likely to never reach steady state during operation. From the scheduling perspective, this means that the dynamics of the process and the closed-loop dynamic characteristics associated with the implemented process control system must be explicitly accounted for in the scheduling calculations [8].

The key impediments towards representing process dynamics in scheduling calculations are, (i) model size (with the models of chemical processes being typically very high dimensional) and, (ii) model nonlinearity (a consequence of capturing the complex phenomena occurring in a chemical plant). In our past work, we addressed the former challenge by introducing the concept of a Scale-Bridging Model (SBM) [31,32,8], as a low-order representation of the scheduling-relevant, closed-loop process dynamics. The name reflects the purpose of the model, that is, to bridge the gap in time scales between the scheduling and control layers of the decision hierarchy (Fig. 1). SBMs typically capture the dynamic response of scheduling-relevant variables (model outputs) to setpoint/target changes imposed by the scheduling mechanism (model inputs). SBMs can adopt a variety of functional forms and can be derived from either full-order process models [33–36] via model reduction or from historical operating data using system identification techniques.

In order to accurately represent the process dynamics, the SBMs utilized thus far in our work were nonlinear. Thus, while reducing model dimensionality, the use of SBMs still leads to a DR scheduling problem that is in a mixed integer nonlinear program (MINLP) format, with all the associated solution challenges. In this paper, we discuss linear reformulations of a specific class of data-driven SBMs, with the goal of recasting the scheduling problem as a MILP.

The solution of the MILP provides the optimal setpoint sequence for the process control system over a relevant time horizon over which actual or predicted electricity prices are assumed to be available, as well as an inventory management solution. The latter consists of the time-resolved flow rates of material leaving or entering the storage system.

The following sections will define mathematically the scheduling problem as well as the modeling approach, as it pertains to the operation of the ASU.

3.2. Representation of time

In order to capture the discrepancies between the scheduling time scale and the time scale of the process dynamics, we utilize two separate time grids (Fig. 3). For the scheduling problem, we rely on a slot-based formulation, with N_I slots, each representing an hour in the scheduling time horizon. This is motivated by the hourly changes in electricity prices, and can be altered as needed. Within each scheduling slot there exists a finer grid, featuring N_J time intervals, which serve to represent the discretized process dynamics as we will describe below. The length of the scheduling slot, $T_I = 1$ hour, is an integer multiple of the dynamic time-step length, or sample time, T_J (min):

$$T_I = \frac{1}{\alpha} N_J T_J \tag{1}$$

The parameter α is a dimensionless conversion factor used to translate between the time units of the scheduling and dynamics time-steps (in this case, $\alpha = 60$). Relations are available for determination of sampling time based on the dominant time constant (τ_{dom}) such as [37, p. 319]:

$$0.01 \leqslant \frac{T_J}{\tau_{dom}} \leqslant 0.05 \tag{2}$$

Fig. 3 illustrates the time grid structure.

As illustrated in Fig. 3, production target/setpoint changes can (but are not required to) occur at each scheduling time slot, *i*. The discretized process dynamics are described in on a finer time grid denoted by time points *j*.

3.3. Scheduling problem formulation

The goal of the optimal scheduling calculation in this work is to minimize operating cost for an ASU operating in an hourly electricity market with prices known (or accurately estimated) 72-h in advance by varying the production rate target/setpoint, u_i:

$$\begin{aligned} &\min_{u_i} \; C = \sum_i \sum_j \mathscr{P}_{i,j} Price_i \\ &\text{s.t.} \\ &\text{Storage system model} \\ &\text{Process dynamic models} \\ &\text{Process Constraints} \\ &\text{Energy price information} \end{aligned} \tag{3}$$

Problem (3) aims to minimize total operating cost over the considered time horizon, under constraints related to process dynamics, product flow rate and quality, and process safety. Starting from this general form, we discuss the models of the different components of the plant, and revisit the scheduling problem formulation in more detail later in the paper.

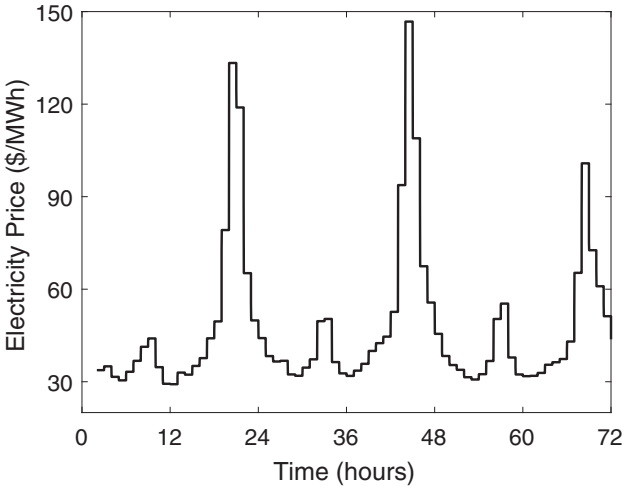

Fig. 2. 3-day electricity prices from CAISO [4] for Oct 16–18, 2017.

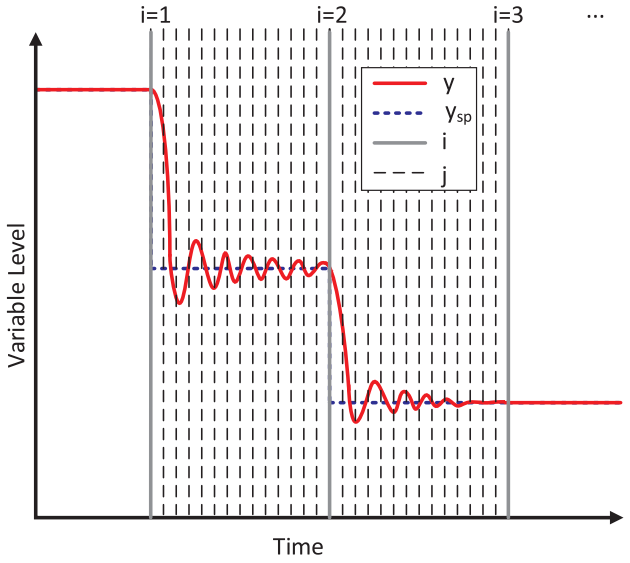

Fig. 3. Time slot formulation showing scheduling slots i, discretization time points, j, for the dynamic model, and the variable y with setpoint y_{sp}.

4. Process model

4.1. Air separation unit

The ASU studied herein is described in Fig. 4, where a single cryogenic distillation column is used to produce high-purity nitrogen gas, supplied continuously via pipeline to industrial users. In the remainder of this section, the dynamic first-principles model of the plant is described, following closely the work of Johansson [38].

1. **Compressor and Turbine Models**: The inlet air stream is compressed to 6.8 bar. The compressor is a key driver of electricity consumption within this process; consumption is partially offset by the power produced by the turbines, which are coupled with generators. The dynamics of the compressors, turbines, and generators are assumed to be fast, and these units are modeled using steady-state expressions. The power demand of the compressor ($\mathscr{W}^{C}$) and the power generation by the turbines ($\mathscr{W}^{t_1}$ and $\mathscr{W}^{t_2}$) are calculated under the assumption that transformations occurring in these systems are polytropic with corresponding efficiencies and head [40].
2. **Primary Heat Exchanger (PHX) Model**: Exiting the compressor, the inlet air stream passes through a brazed-aluminum plate-fin Primary Heat Exchanger (PHX) [39], where it is liquefied. Prior to liquefaction, part of the air stream is removed from the heat exchanger and passed through a turbine to generate additional refrigeration. The PHX model is therefore divided into two zones (Fig. 4), which are discretized lengthwise to account for the heat exchange between the hot and cold streams, and the aluminum walls.
3. **Distillation Column Model**: Following the PHX, the liquefied air stream enters the cryogenic distillation column.The model for the distillation column is based on the work of Huang et al. [41], whereby the following assumptions are made: (i) each stage is well-mixed, (ii) the vapor phase behaves as an ideal gas, (iii) vapor-liquid equilibrium (VLE) is reached on each stage, and (iv) there is no heat loss throughout the column. The 30-stage column has a condenser with an operating pressure of 6.4 bar and a pressure drop of 0.2 bar. An activity model is used to model phase equilibrium on each stage, with activity coefficients determined by the Margules equation [42] and the saturated vapor pressure computed using Antoine's equation [43].
4. **Integrated Reboiler/Condenser Model**: The reboiler/condenser for the column is integrated, utilizing the liquid in the bottoms (expanded adiabatically to 2.5 bar) to condense the vapor from the top of the column. The model for this component is adapted from [39], with the following assumptions: (i) no consideration of material/energy accumulation (i.e. fast dynamics) on the coolant side, (ii) the condensed liquid is saturated, (iii) the heat duty required to condense the vapor stream is supplied entirely by the reboiler, and (iv) the outlet liquid composition matches the composition of the inlet vapor at the top of the column. For simplicity, the reboiler is modeled as an equilibrium stage with additional heat input (from the condenser).

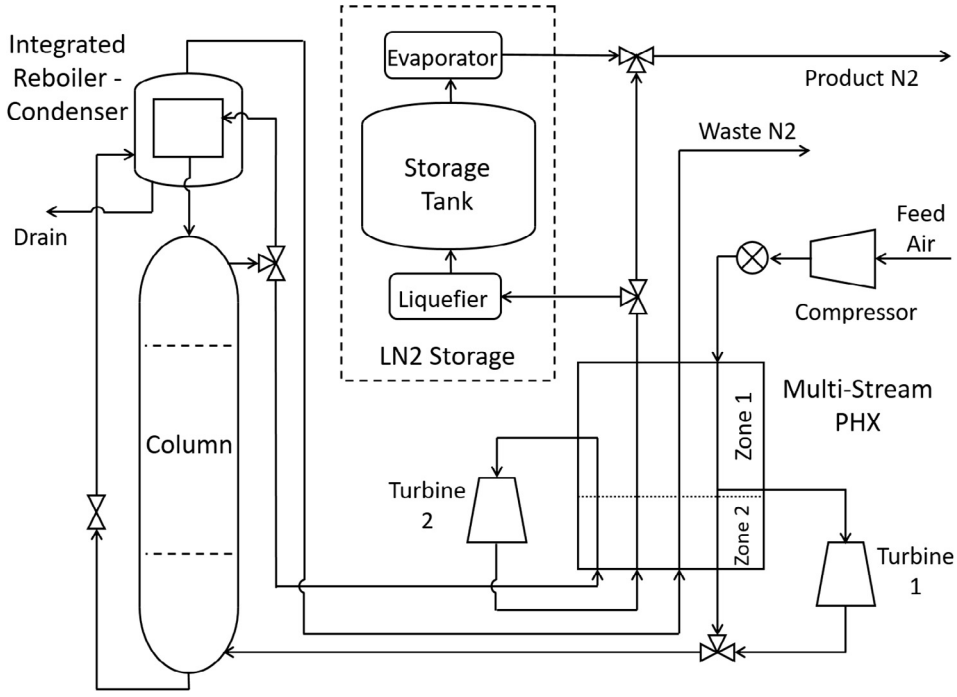

Fig. 4. Cryogenic ASU for N_2 production [19,39].

5. **Liquefier and Inventory System Model**: We consider that the liquefier operates at constant efficiency (here assumed to be 80%), and its power consumption ($\dot{W}^{L}$) is computed based on the net work of the turbine and compressor. Conversely, an evaporator is used to vaporize the liquid and obtain nitrogen gas to be delivered to customers when the plant production drops below demand. The evaporator is assumed to operate at ambient conditions using no additional power. The liquefier dynamics are assumed to be fast and any internal holdups to be negligible.
The liquid storage system is described by a material balance consisting of a first-order differential equation for the holdup, and associated depletion and capacity constraints:

$$\frac{ds}{dt} = f_s^{in}(t) - f_s^{out}(t) \tag{4a}$$

$$f_s^{in}(t) = f_s^{out}(t) + F^p(t) - D(t) \tag{4b}$$

$$f_s^{out}(t) = D(t) - F^p(t) \tag{4c}$$

Using the time grid defined in Section 3.2 and a forward Euler discretization, this model can be written in discrete time in the following form:

$$s_{i,j} = T_J\left(f_{s_{i,j}}^{in} - f_{s_{i,j}}^{out}\right) + s_{i,j+1} \tag{5a}$$

$$s_{i,1} = s_{i-1,N_j} \tag{5b}$$

$$f_{s_{i,j}}^{in} = f_{s_{i,j}}^{out} + F_{i,j}^p - D_{i,j} \tag{5c}$$

$$f_{s_{i,j}}^{out} = D_{i,j} - F_{i,j}^p \tag{5d}$$

where $D_{i,j}$ is nitrogen demand rate, $s_{i,j}$ is the inventory holdup, $F_{i,j}^p$ is the production rate, and $f_{s_{i,j}}^{out}$ and $f_{s_{i,j}}^{in}$ represent the flow rates of the streams leaving and entering the storage system, respectively. A continuity condition, (5b) is necessary when discretizing (4) such that the storage holdup at the end of scheduling slot $i-1$ is equal to that at the beginning of slot i. In the case study considered here, we assume that the demand is known and constant in time ($D = 20$ mol/s). The plant is capable of altering its operation, whereby the production rate can change by $\pm$ 20% of its nominal production rate (which is assumed to be identical to the demand rate). Hence, only $F_{i,j}^p$ needs to be modeled to calculate $f_{s_{i,j}}^{out}$ and $f_{s_{i,j}}^{in}$ using (5).

The overall plant model is a Differential Algebraic Equation (DAE) system comprising 6094 equations, of which 430 are differential.

4.2. Plant power demand

The electricity consumption/production of/by the compressors/turbines ($W_{i,j}$) is assumed to be directly proportional to the flow of material through each unit. The feed stream passes through both the compressor (C) and Turbine 1 (T_1), while the product stream, of flowrate $F_{i,j}^p$, flows through Turbine 2 (T_2) and the feed stream to the storage system, $f_{s_{i,j}}^{in}$, passes through the liquefier (L).

$$\begin{aligned}
\dot{W}_{i,j}^{C} &= \Omega_C F_{i,j}^f \\
\dot{W}_{i,j}^{t_1} &= \Omega_{t_1} F_{i,j}^f \\
\dot{W}_{i,j}^{t_2} &= \Omega_{t_2} F_{i,j}^p \\
\dot{W}_{i,j}^{L} &= \Omega_L f_{s_{i,j}}^{in}
\end{aligned} \tag{6}$$

The parameters Ω are set based on the polytropic head for each unit, and are assumed to be constant and independent of the production rate. The variable $f_{s_{i,j}}^{in}$ can be calculated from $F_{i,j}^p$ using (5), and therefore the only additional variable needed to model power use by the plant is the feed flowrate, $F_{i,j}^f$.

Based on the above, the (time-varying) power requirements for the entire plant ($\mathscr{P}_{i,j}$) are computed as:

$$\mathscr{P}_{i,j} = \dot{W}_{i,j}^{C} + \dot{W}_{i,j}^{L} - \dot{W}_{i,j}^{t_1} - \dot{W}_{i,j}^{t_2} \tag{7}$$

where $\dot{W}_{i,j}$ represents the net work of each unit, calculated by Eq. (6). The power demand of the ASU (7) factors directly into the operating cost:

$$Cost = \sum_i \sum_j \mathscr{P}_{i,j} Price_i \tag{8}$$

where $Price_i$ is the vector of time-based electricity prices in Fig. 2.

Remark 1. The efficiencies of the liquefier and rotating machinery (turbines, compressor) used in the plant are, in practice, not constant throughout the operating range [30]. While capturing efficiency fluctuations as a function of flow would not pose a significant computational challenge in our framework, the assumption of constant efficiency (constant Ω) is reasonable in this case: the process operates at constant pressure between production rate changes and we assume that inlet temperatures do not change significantly [38]. Assuming constant efficiencies also makes the results of the case study more transparent. Specifically, economic benefits can strictly be attributed to the DR scheduling strategy.

4.3. Scheduling-relevant variables

Pattison et al. [8] made the key observation that not all members of the set of process variables (whose dimensionality exceeds several thousand, as pointed out above) are relevant to production scheduling calculations. Following the rationale presented by Pattison et al. [8], we define the subset of variables relevant to scheduling calculations as those which are at or near their bounds (or are part of the definition of constraints that are active) during either steady-state operation or during transition. In the case of a complex process such as air separation, multiple constraints are likely to exist to maintain performance, efficiency, and safety. However, only a subset of these constraints may be at risk of being violated, and the identification of this subset can substantially reduce the number of variables which should be captured in the scheduling model (in addition to the model of the inventory system described above), thereby reducing the scheduling problem size. This determination can be made based on analyzing closed loop historical operating data, which are typically available in practical situations.

The set of scheduling-relevant variables typically includes:

- Variables present in the scheduling objective function. In this work, the objective consists of the operating cost over the full 72-h time horizon (8). Given that $f_{s_{i,j}}^{in}$ is readily calculated from production rate $F_{i,j}^p$ (5), the two variables required to evaluate the cost function are $F_{i,j}^p$ and $F_{i,j}^f$ (6).
- Variables Relevant to Process and Quality Constraints (PCs and QCs). Active constraint identification was carried out by observing a set of simulation data (described later). The PCs and QCs for this ASU as identified in [8] are discussed, including the variables

relevant to each QC and PC:

– *QC1*: Demand must be met throughout the time horizon–the total production must be greater than or equal to the demand. In this case, the production flow rate, $F^p_{i,j}$, can be supplemented by the flow of product from storage, $f^{out}_{s_{i,j}}$, (5).

– *QC2*: Product impurity levels must remain below the maximum allowed value ($I_{max} = 2000$ ppm). The impurity levels (I^p_{ij}) are defined based on the mole fraction of O_2 in the product stream.

$$I^p_{i,j} \leqslant I_{max} \quad \forall \ \{ij\} \tag{9}$$

This constraint is critical, therefore a "backoff" (i.e., a stricter limit) of $I'_{max} = 1800$ ppm is used to account for model inaccuracies. Such stricter constraints are utilized routinely in practice to maintain feasible operation [44,45].

– *PC1*: The reboiler holdup at the end of the time horizon ($M^r_{N_I,N_J}$) should be greater than or equal to the level at the beginning of the time horizon ($M^r_{1,1}$). This process constraint (10) is imposed to ensure that refrigeration within the process is not depleted. In addition, the reboiler holdup is bounded such that it is greater than 70 kmol and less than the maximum capacity, $M^r_{max} = 120$ kmol.

$$M^r_{N_I,N_J} \geqslant M^r_{1,1} \tag{10}$$

– *PC2*: The air stream exiting zone 2 of the PHX must be in the liquid phase, therefore the outlet pressure ($P^{zone2}_{i,j}$) must be greater than the bubble point pressure ($P^{bub}_{i,j}$). The relation below is used to enforce this constraint:

$$P^b_{i,j} = \frac{P^{zone2}_{i,j}}{P^{bub}_{i,j}} \geqslant 1.05 \quad \forall \ \{ij\} \tag{11}$$

– *PC3*: Streams in zone 1 of the PHX must be in the gas phase. In zone 1 of the PHX, only sensible heat is removed from the inlet air stream, which is constrained to be in the vapor phase at all times such that no phase transformations occur within zone 1. Therefore, outlet pressure P_{zone1} should be lower than the dew pressure at the air outlet ($P^{dew}_{i,j}$), as enforced by the constraint below:

$$P^d_{i,j} = \frac{P^{zone1}_{i,j}}{P^{dew}_{i,j}} \leqslant 0.96 \quad \forall \ \{ij\} \tag{12}$$

– *PC4*: There is no flooding in the distillation column. Flooding occurs when vapor flow rate is excessively large, causing liquid from a stage to flow upwards. Flooding reduces stage efficiency and increases the pressure drop across the column. The constraint below is based on Sinnott [46] and Cao et al. [39]:

$$\delta^f_{nij} = \frac{v_{nij}}{v^{flood}_{nij}} \leqslant 0.97 \quad \forall \ \{nij\} \tag{13}$$

Vapor velocity at tray n is represented by $v_{n,i,j}$ and flooding velocity is given by $v^{flood}_{n,i,j}$. Detailed velocity calculations are described by Johansson [38]. In an effort to reduce the number of model variables, we represent $\delta^f_{n,i,j}$ with $\delta^{f(max)}_{i,j}$ because flooding typically happens simultaneously on the trays in the column which tend to flood.

– *PC5*: The temperature driving force across the reboiler/condenser must be greater than a lower limit, ensuring that heat flow occurs in the correct direction, i.e., $Q_{i,j} = U_{i,j}A(T^{cond}_{i,j} - T^{reb}_{i,j}) \geqslant 0$.

$$\Delta T_{i,j} = T^{cond}_{i,j} - T^{reb}_{i,j} \geqslant \Delta T_{min} \tag{14}$$

The minimum approach temperature, ΔT_{min}, is 1.9 °C, with a "backoff" constraint set at 2. 01 °C.

– *PC6*: In order to ensure that stored material is not depleted during operation, it is necessary to impose a constraint such that the holdup in the storage system at the end of the time horizon is greater than or equal to the holdup at the beginning of the time horizon.

$$s_{N_I N_J} \geqslant s_{1,1} \tag{15}$$

A backoff constraint of $s_{1,1} + 2$ kmol was used to ensure the endpoint storage constraint was met. Note that this constraint should be adjusted to prevent unecessary accumulation of material in the case when the framework described later in the paper is applied repeatedly, e.g., in a moving horizon fashion. In addition, the storage holdup is bounded such that it is greater than zero and less than the maximum capcity, $s_{max} = 200$ kmol.

The simulations carried out by Johansson [8] demonstrated that PC2 is in effect never in danger of being violated, and as a consequence the set of scheduling-relevant variables used henceforth only includes QC1, QC2, PC1, PC3, PC4, PC5, and PC6.

4.4. Scheduling-oriented Scale-Bridging Models

Du et al. [31] introduced the notion of Scale-Bridging Model (SBM) as a (low-order) representation of the closed-loop dynamics of the process that are relevant to scheduling calculations, that is, of the dynamics of the variables involved in the PCs and QCs. The *input* variables of SBMs are the production target(s) set by the scheduling calculation (in our case, this is the gas nitrogen production rate), while the outputs are precisely the (time-dependent) trajectories of the variables involved in the PCs and QCs.

Based on the discussion above for the ASU, we derive SBM representations for $\overrightarrow{w_{i,j}} = \{F^p_{i,j}, I^p_{i,j}, F^f_{i,j}, M^r_{i,j}, \delta^f_{i,j}, P^d_{i,j}, \Delta T_{i,j}\}$. We note that the sixth scheduling-relevant variable, $s_{i,j}$, can be easily modeled using the DAE system in (5).

SBMs can be derived in several ways and can take several formats. In the original developments described by Du et al. [31], an explicit expression of the closed loop dynamics was available owing to the use of a nonlinear input-output linearizing controller. On the other hand, Pattison et al. [8] advocate the use of data-driven SBMs, obtained from closed-loop operating data via system identification techniques. In this paper, we rely on data driven models, and consider two widely-accepted model classes: (nonlinear) Hammerstein Wiener (HW) models, and (linear) finite step response (FSR) models.

In order to identify HW and/or FSR models for the ASU, we generated a training data set. The data generation process comprised two separate steps: (i) computing a DR production schedule based on a *static* model of the ASU, which links hourly power consumption to production rate based on a simplified efficiency model (with additional rate-of-change constraints limiting the allowable change in production targets between consecutive hours) and, (ii) simulating this schedule using the full-order plant model described above. The resulting data exhibited several constraint violations (notably, product purity constraints), but were considered useful for the purpose of model identification. We note that the models were identified in a previous work by Pattison et al. [8], which assumed a Texas plant location and therefore utilized Texas electricity prices.

4.4.1. Hammerstein-Wiener (HW) models

HW models are nonlinear data-driven input/output models which consist of a linear dynamic component with nonlinear input

Fig. 5. General HW model form.

$(H(u))$/ouput$(W(y))$ functions (Fig. 5) [47, p. 30–32].

The variable u represents the system inputs, y is the output of the linear dynamic block, and w is the output variable.

$$\begin{aligned} h &= H(u) \\ \frac{d\vec{x}}{dt} &= A\vec{x} + Bh \\ y &= C\vec{x} \\ w &= W(y) \end{aligned} \tag{16}$$

In the case of the SBMs developed for the ASU, u is invariably the production rate setpoint provided by the scheduling calculation, while w represents variables pertaining to either PCs or QCs. HW models for this the ASU were previously identified by Pattison et al. [8], in particular for $\vec{w}^{HW} = \{I^p, M^r, \delta^f, P^d, \Delta T\}$, which were reformulated in this work. Model specifics are provided in Table 1, where model accuracy was determined using the Normalized Mean Square Error (NMSE):

$$NMSE = 1 - \frac{||w^{ref} - w||}{||w^{ref} - mean(w^{ref})||} \tag{17}$$

4.4.2. Finite Step Response (FSR) models

The remainder of the scheduling-relevant variables ($\vec{w}^{FSR} = \{F^p, F^f\}$) were represented using FSR models. FSR models are data-driven non-parametric models, and have gained acceptance for representing the dynamics of process systems, particularly when the dynamics are complex, and the exact model order and time delay are unknown. The general FSR model form is given below [37, p. 128–129]:

$$w_{i,j+1} = w_{i,j=0} + \sum_{n=1}^{J-1} [S_n \Delta u_{i,j-n+1}] + S_J u_{i,j-J+1} \tag{18}$$

Embedding models of the type (18) in scheduling calculations presents the advantage of adding a set of linear constraints. However, this additional constraint set may in effect be quite high dimensional (i.e., n in (18) can be quite large). Thus, we develop SBMs using the FSR structure only for variables whose dynamics are quite fast; the heuristic we propose here is that FSR representations are suitable for variables whose *settling time* is shorter than the duration of the scheduling time slot. Equivalently, we request that a variable reach steady state after *each* change in setpoint imposed by the scheduling layer. Furthermore, $\Delta u_{i,j} = 0$ when $1 < j < N_J$, and (18) therefore reduces to:

$$w_{i,j} = w_{i-1,j} + S_j(u_i - u_{i-1}) \tag{19}$$

where the coefficients S_j are used to estimate the value of $w_{i,j}$ at time step i based on $w_{i-1,j}$ and the change in set-point Δu_i.

For the ASU case study, we identified FSR models for the remaining (i.e., not described by HW models) variables. Table 2 provides details for the resulting models. The trapezoid rule was used to approximate the integrals for determining %fit, using:

$$\%Fit = 100\frac{\int w_{i,j}^{ref} - \int w_{i,j}}{\int w_{i,j}^{ref}} \tag{20}$$

Fig. 6 show $F_{i,j}^p$ and $F_{i,j}^f$ compared to the training data. As shown, the FSR models are able to map the trajectory of the full-order model accurately, only slightly over/under estimating $F_{i,j}^p$ and $F_{i,j}^f$ at the maximum and minimum operating points.

Table 2
FSR model statistics, where % fit is relative to the full-order model [38] training data.

Variable	Type	Sample Time (min)	% Fit
$F_{i,j}^p$	FSR	1	99.87
$F_{i,j}^f$	FSR	1	99.96

5. Linear reformulations of Scale-Bridging Models

The use of SBMs reduces the dimension of the DR scheduling problem (3) considerably and, along with it, the requisite time for computing a solution [8]. Nevertheless, it is important to note that SBMs in HW format are still nonlinear, and the resulting problem is a mixed-integer nonlinear program. We make note that FSR models as defined in Section 4.4.2 are already amenable to solution in an MILP framework.

In this section, we define a novel set of linear reformulations for HW models, with the ultimate goal of expressing the DR scheduling problem as a mixed-integer *linear* program (MILP). The motivation for this development is twofold: first, a MILP formulation allows us to use powerful, proven commercial solvers to obtain solutions with optimality guarantees. Second, in view of future developments concerning embedding chemical process representations in *grid-level* scheduling models, it is preferable (and in many cases required) to rely on linear model forms.

To this end, we begin by assuming that the input and output functions $H(u)$ and $W(y)$ are piecewise linear [48]. Based on this assumption, these functions can be reformulated as a set of mixed-integer linear constraints using special ordered sets of the second type (SOS2) – an approach commonly used to reformulate piecewise linear *objective functions*, but which we employ for the reformulation of constraints.

Considering specifically the input nonlinearity $H(u)$, an expression for the output $h_i = H(u_i)$ is computed by comparing the value of u_i to the breakpoints, $bp_{i,k}^H$, then performing a linear interpolation (using $\lambda_{i,k}^H$) between the corresponding values of $H(u_i)$, $pw_{i,k}^H$ (Fig. 7). The binary variable $z_{i,k}^H$ ensures that only one interval (i.e., two adjacent breakpoints) are active at any time step i.

$$\sum_k \lambda_{i,k}^H = 1 \tag{21a}$$

$$\lambda_{i,k}^H \leqslant z_{i,k}^H \tag{21b}$$

$$\sum_k z_{i,k}^H = 2 \tag{21c}$$

$$z_{i,k}^H + z_{ik'}^H \leqslant 1 \quad \forall\, k' > k+1 \tag{21d}$$

$$z_{i,k}^H \in \{0,1\} \tag{21e}$$

SOS2 variables are natively supported by many algebraic modeling environments, and are defined such that two adjacent $\lambda_{i,k}^H$ must be nonzero (active) (21) and therefore act as weighting variables for linear

Table 1
HW model dimensions from [8], where NMSE stands for Normalized Mean Square Error.

Variable	$H(u)$ breakpoints	Linear state-space system order	$W(y)$ Type	$W(y)$ Order	$W(y)$ breakpoints	NMSE (training)	NMSE (validation)
I^p	4	4	Piecewise linear	N/A	6	0.82	0.52
M^r	3	4	Polynomial	1	N/A	0.78	0.75
δ^f	5	5	Polynomial	2	N/A	0.91	0.92
P^d	2	8	Polynomial	2	N/A	0.83	0.97
ΔT	9	4	Piecewise linear	N/A	6	0.69	0.84

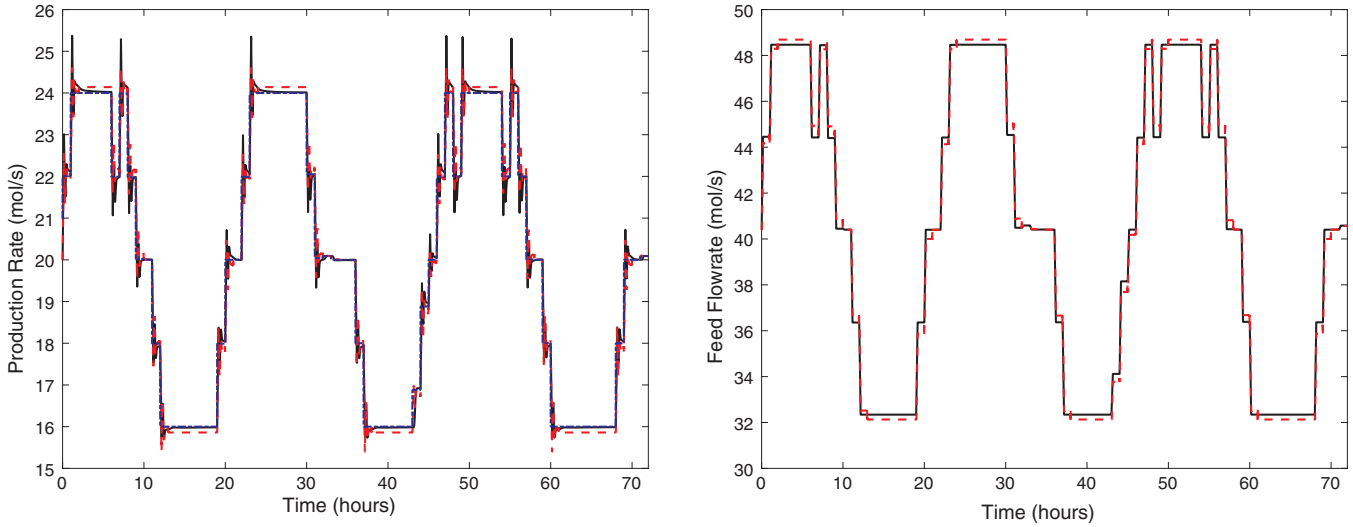

Fig. 6. Plots comparing MILP FSR models (red dashed) to the full-order model output (black solid) over the set of training data set-points (blue dashed-dot) for a 72 h time horizon. (For interpretation of the references to colour in this figure legend, the reader is referred to the web version of this article.)

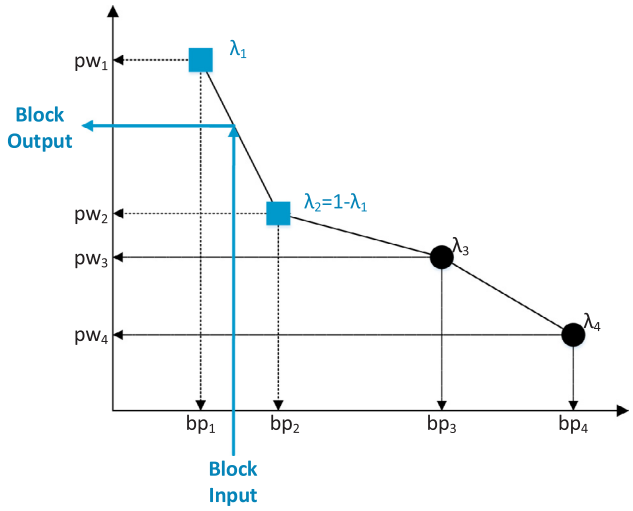

Fig. 7. Reformulation of the nonlinear Hammerstein block $H(u)$.

interpolation (22).

$$u_i = \sum_k [\lambda^H_{i,k} bp^H_{i,k}] \tag{22a}$$

$$h_i = \sum_k [\lambda^H_{i,k} pw^H_{i,k}] \tag{22b}$$

The piecewise linear output functions $W(y)$ can be dealt with in a similar way:

$$\sum_k \lambda^W_{i,j,k} = 1 \tag{23a}$$

$$\lambda^W_{i,j,k} \leqslant z^W_{i,j,k} \tag{23b}$$

$$\sum_k z^W_{i,j,k} = 2 \tag{23c}$$

$$z^W_{i,j,k} + z^W_{i,j,k'} \leqslant 1 \quad \forall\, k' > k+1 \tag{23d}$$

$$z^W_{i,k} \in \{0,1\} \tag{23e}$$

the output values $w_{i,j}$ can be computed via linear interpolation using output breakpoints $bp^W_{i,j,k}$ and the values of $W(y_{i,j})$ $(pw^W_{i,j,k})$ at these breakpoints:

$$y_{i,j} = \sum_k [\lambda^W_{i,j,k} bp^W_{i,j,k}] \tag{24a}$$

$$w_{i,j} = \sum_k [\lambda^W_{i,j,k} pw^W_{i,j,k}] \tag{24b}$$

An example of this linearization is depicted in Fig. 7.

We assume that the dynamic block in the HW structure is a linear state-space form. Using this model in the time representation described in Section 3.2 requires that it be converted to discrete time. This can be accomplished in a number of ways; in this work, we employ a zero-order hold, where the sampling times are integer divisors of the scheduling time slot length, and are determined using (2). Index j therefore denotes a separate discretization time grid for the dynamics of each of the scheduling-relevant variables. We note that the same sampling time can be used for all the models, but choosing dedicated, individual sampling times is computationally more efficient.

The general structure of the resulting (discrete-time) HW model thus becomes:

$$\begin{aligned} h_i &= H(u_i) \\ \vec{x}_{i,j+1} &= A\vec{x}_{i,j} + Bh_i \\ y_{i,j} &= C\vec{x}_{i,j} \\ w_{i,j} &= W(y_{i,j}) \end{aligned} \tag{25}$$

An additional continuity condition is necessary for correctly capturing the dynamics of the state variables between scheduling intervals; in particular, we must enforce that the value of each state variable at the beginning of scheduling slot i be the same as its value at the end of the previous scheduling time slot $i-1$:

Table 3
Comparison of the response of the linearized HW and nonlinear HW models identified by Pattison et al. [8]) for the training data set).

Variable	Sample time (min)	% Fit
$I^p_{i,j}$	6	98.70
$M^r_{i,j}$	2	99.99
$\delta^f_{i,j}$	10	99.63
$P^d_{i,j}$	10	99.97
$\Delta T_{i,j}$	6	99.80

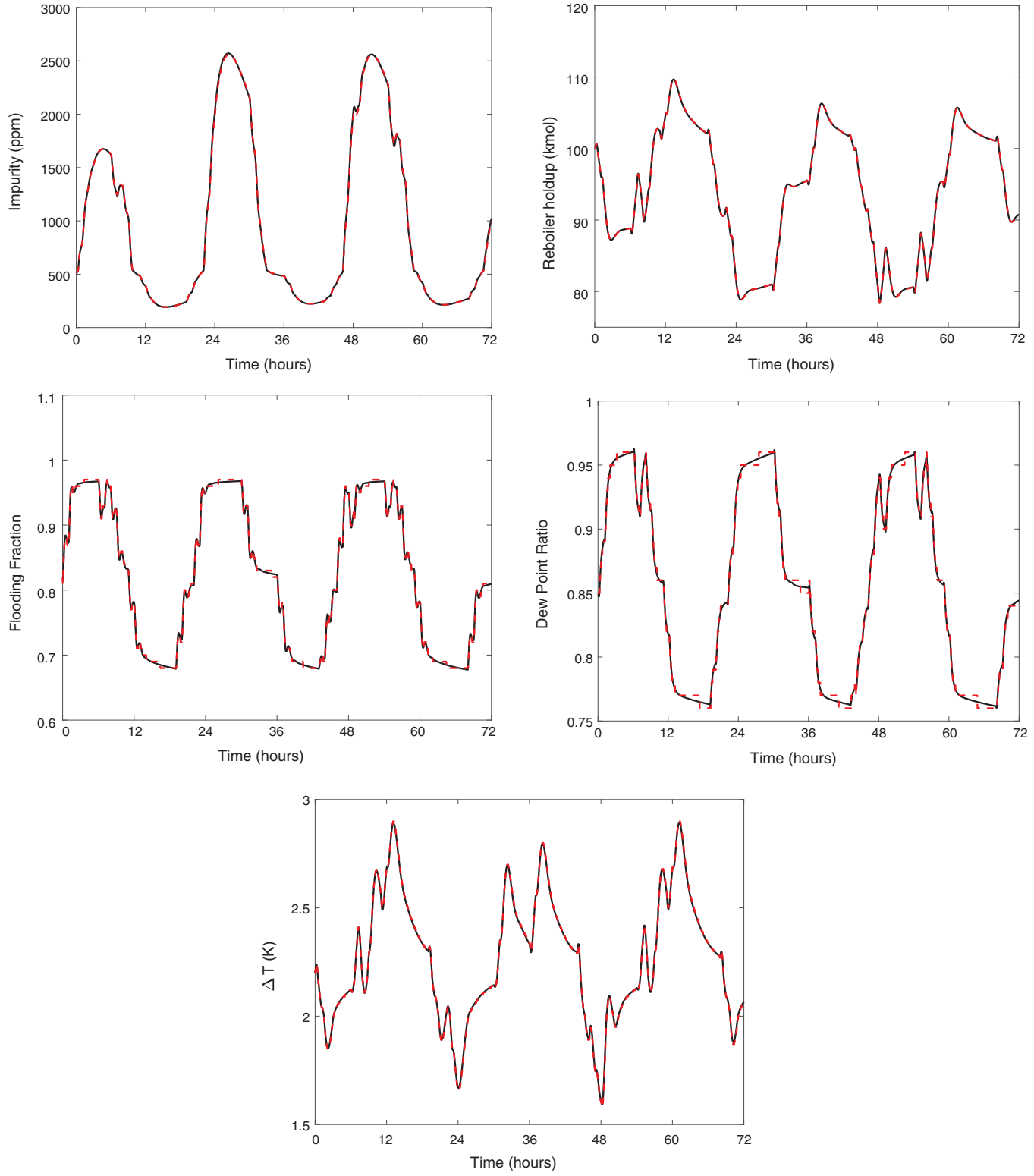

Fig. 8. Transient simulation of the response of nonlinear (black solid) vs. linearized HW models (red dashed) for the training data set. (For interpretation of the references to colour in this figure legend, the reader is referred to the web version of this article.)

$$\vec{x}_{i,1} = \vec{x}_{i-1,N_j} \tag{26}$$

This discretization strategy was applied to the HW models described in Section 4.4.1, and the response of the resulting linearized models was compared to the response of the original (nonlinear) HW models; the results are presented in Table 3.

Fig. 8 presents the simulated response of the two models for the training data set, demonstrating that the linearized versions of the HW models are an accurate representation of their NL counterparts. Further, we note that under the current assumptions, this linear reformulation is, in fact, exact, with the discrepancies originating in the discretization of the continuous-time dynamics. We also note that carrying out a

simulation using the discretized and reformulated HW model (25) calls for the solution of a mixed-integer linear optimization problem; we found that this simulation problem can be solved very efficiently (in a matter of a few seconds) using CPLEX 12 [49] in GAMS [50].

Remark 2. A further simplification of the constraint system associated with the linearized HW models is possible in the case where the exact value of the output $w_{i,j}$ is not needed and, rather, we are interested in ensuring that the variable $w_{i,j}$ remains within some specified lower and upper bounds. This is the case for, e.g., variables $\Delta T_{i,j}$,$\delta^f_{i,j}$,$P^d_{i,j}$, and $I^p_{i,j}$ in $\overrightarrow{w}^{HW}_{i,j}$ (for which bounds are specified in (14), (13), (12), and (9), respectively). For these variables, the exact trajectories are not of concern as long as the values at any point in time are not outside the specified bounds. This observation then leads to the conclusion that the output nonlinearity W can be represented as a linear function, using two breakpoints corresponding to the upper and lower bounds of the variable.

This simplification does not apply to, i) variables that are included in the cost function, or to variables for which the exact value must be known (e.g., $M^r_{i,j}$, which is included in the endpoint constraint (10)). This simplification can reduce the number of binary decision variables present in the optimization problem (note that the number of binaries used to discretize the output nonlinearity W is $\mathcal{O}(N_J)$ times higher than the number of binaries associated with the input nonlinearity H, since the output of W must be calculated at every time point i,j in the time grid (rather than once every scheduling slot i, as is the case for H).

6. MILP Formulation of DR scheduling problem

6.1. Problem formulation

The problem up to this point consists of low-order scale bridging HW or FSR models representing the subset of scheduling-relevant variables previously identified, $\overrightarrow{w}_{i,j} = \{F^p_{i,j},I^p_{i,j},F^f_{i,j},M^r_{i,j},dT_{i,j}\}$. The problem structure is block angular, where an overarching "common problem" contains the objective function (8), which is the total operating cost over the entire time horizon. This common problem is complemented by hourly "sub-problems" linked together by the continuity constraints (26). The problem structure is depicted in Fig. 9.

Given the formulation discussed thus far, the resulting optimization problem (P1) is given:

$$\min_{u_i} \quad C = \sum_i \sum_j \mathscr{P}_{i,j} Price_i$$

s.t.
Process model (25),19
Inventory model (5)
Initial Conditions
Continuity Conditions (26)
Process Constraints (PC1, PC3, PC4, PC5, PC6)
Quality Constraints (QC1, QC2) (27)

P1 has 86,643 variables, 1512 of which are integers.

6.2. Decomposition-based solution strategy

In examining the block-angular structure in Fig. 9, the complicating constraints can be identified as the continuity constraints (26) associated with the use of discrete HW models (25) and the differential storage model (5), of which there are 1872.

The solution of this problem lends itself naturally to a Lagrangian Relaxation (LR) approach, where the continuity conditions given by (26) are dualized, and an iterative scheme is used to reduce constraint violations until a specified threshold is reached [51] (Fig. 10). The initial values of the stepsize, the Lagrange Multiplier, and the constraint violations are determined by solving P1 as a Relaxed MILP (RMILP) without the continuity conditions (26).

Based on the above, a more computationally efficient relaxed subproblem, hereafter referred to as P2, is defined below and used to calculate the optimal hourly schedule of production set point changes.

$$\min_{u_i} \quad L_m = C_m + \sum_i LD_{i,m}\gamma_{i,m}$$

s.t.
Process model (25,19)
Inventory model (5)
Initial Conditions
Process Constraints (PC1, PC3, PC4, PC5, PC6)
Quality Constraints (QC1, QC2) (28)

P2 has 91,837 variables, 1512 of which are integers. The parameter $\gamma_{i,m}$ reflects the linear formulation of the absolute value of the continuity constraint violation for state variable $x_{i,j}$ at each scheduling time step for LR iteration m. We note that the absolute value is used to ensure that constraint violations are nonnegative when applied to the above minimization problem, P2.

$$x^{pos}_{i,m} - x^{neg}_{i,m} = x_{i,1,m} - x_{i-1,N_J,m} \tag{29a}$$

$$x^{pos}_{i,m}, x^{neg}_{i,m} \geqslant 0 \tag{29b}$$

$$\gamma_{i,m} = x^{pos}_{i,m} + x^{neg}_{i,m} \tag{29c}$$

The stepsize for LR iterations is calculated based on $\gamma_{i,m}$, where ϵ is a small number added to prevent division by zero, θ is a scalar initially set to 2, reduced by half if there is no improvement between iterations. The stepsize calculation is given below, where the calculation is repeated for each iteration, m, needed [52] [53, p. 530].

$$Stepsize_{i,m} = \theta \frac{L_m - C_m}{\epsilon + ||\gamma_{i,m}||_2} \tag{30}$$

with the Lagrangian multiplier ($LD_{i,m}$) acting as a penality term, calculated by:

$$LD_{i,m} = \max(0, LD_{i,m-1} + Stepsize_{i,m}\gamma_{i,m}) \tag{31}$$

The iterations terminate once a specified tolerance is met. We use the relation below to determine convergence, since it uses both the constraint violations, $\gamma_{i,m}$, and the optimality gap between the lower bound $Dual_m$ and the current cost, $Cost_m$.

$$|LD_{i,m-1} - LD_{i,m}| \leqslant \epsilon \tag{32}$$

We note that LR (in this case) updates the lower bound based on the

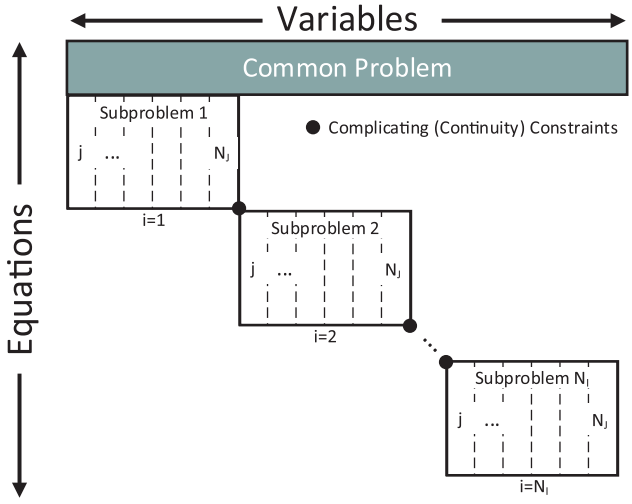

Fig. 9. Structure of the DR scheduling problem.

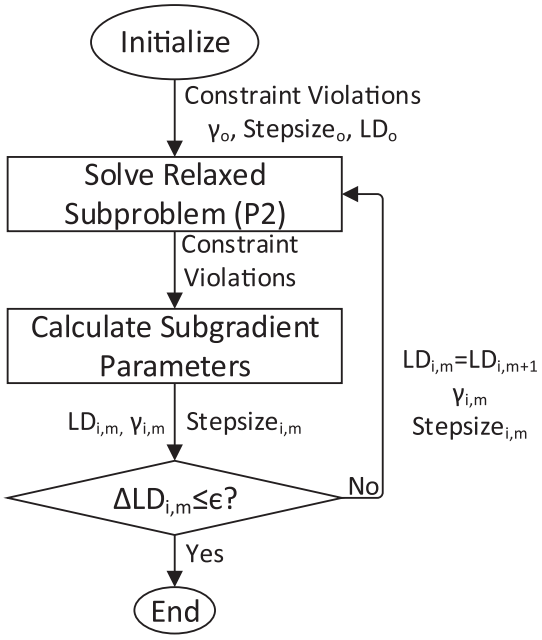

Fig. 10. Lagrangian Relaxation with sub-gradient iterations algorithm, where index *i* represents the scheduling time steps and index *m* represents the iteration number.

constraint violations. An upper bound on the objective was set empirically at a static value 10% higher than the 3-day operating cost where no DR is used. Given that the complicating constraints are equality constraints, the solution of P2 can be guaranteed to be globally optimal for P1 as long as there is a feasible solution to the primal problem, P1, i.e. the complicating (continuity) constraints can be met [54, p. 82–114], [55,9, p. 277–283]. In other words, when the continuity constraints are met (i.e., $\gamma_{i,m} = 0$), problem P1 and P2 are equivalent. Intuitively, the *dynamics* of the system must be *feasible* before any optimality claims on the economic operation can be made. We direct the reader to the works of Geoffrion [54, p. 82–114], Bertsekas [55, p. 277–283], Guignard [56], Rush and Collins [9], and Kelley et al. [48], where the theoretical basis for this finding is discussed.

7. Air separation unit results and discussion

The DR scheduling problem described above was solved without LR (P1) and using the proposed LR approach (P2), each resulting in an optimal sequence of production rate set-points, which were then simulated using a full-order model based on the work of Johansson [38].

For comparison purposes, we also present the results of P3, which consists of solving the DR scheduling problem using the nonlinear HW SBMs as identified by Pattison et al. [8].

$$\min_{u(t)} \quad C = \int_0^{T_m} \mathscr{P}(t) Price(t) dt$$
s.t.
Process model Continuous HW
Inventory model
Initial Conditions
Process Constraints (PC1-PC6)
Quality Constraints (QC1, QC2) (33)

We also include in the comparison the results obtained by using a full-order process model based on the work of Pattison et al. [8], a problem that we refer to as P4.

$$\min_{u(t)} \quad C = \int_0^{T_m} \mathscr{P}(t) Price(t) dt$$
s.t.
Full-order Process model
Inventory model
Initial Conditions
Process Constraint (PC1-PC6)
Quality Constraints (QC1, QC2) (34)

Lastly, we include P5, where the same optimal scheduling problem was solved using a rate-of-change constraint, where the change in production rate set-point between consecutive hours is limited such that the "ramp up" and "ramp down" in production rate is comparatively gradual. A steady-state gain-like model was used, of the format:

$$w_{i,j} = w_{i-1,j} + S_{N_j}(u_i - u_{i-1}) \quad (35)$$

The above captures feed flowrate and production rate, which can then be used to calculate the flow rate of material into storage, $f^{in}_{s_{i,j}}$, with (5), where net work, $\mathscr{W}_{i,j}$, from (6) is used to determine power consumption, $\mathscr{P}_{i,j}$ with (7). This type of model is similar to the FSR model (19) presented previously and uses the final model coefficient, S_{N_j} to represent the assumption that steady-state is instantly achieved for each setpoint change. The maximum allowed hourly rate of change was selected as 0.5 mol/s/h from a range of ramp-rate constraints between 0.1 mol/s and 3 mol/s, where 0.5 mol/s was the highest-possible ramp-rate constraint without quality/safety constraint violations. P5 is formulated as:

$$\min_{u_i} \quad C = \sum_i \sum_j \mathscr{P}_{i,j} Price_i$$
s.t.
Steady-state gain model (35)
Inventory model
Initial Conditions
Process Constraints (PC1, PC6)
Quality Constraints (QC1)
$|u_i - u_{i-1}| \leqslant 0.5$ mol/s/h (36)

In Table 4, we compare the solutions of P1, P2, P3, P4, and P5 in terms of the value of the objective function and solution time. In reporting the results for P1-P5 we also provide the costs predicted by the optimization problem using the low-order models, and the total cost computed from simulating the full-order model. The solutions of P1 and P2 in Table 4 correspond to an optimality gap of 0.053% and 0.040%,

Table 4
Summary of optimal solutions achieved by P1–P5.

Problem	Predicted optimal cost (low-order model) ($)	Actual cost (full-order model) ($)	Savings compared to constant production rate (%)	CPU time (s)	Constraint violations?
P1	1,013.31	1,013.64	1.12	704 (11.7 min)	No
P2	1,013.31	1,013.64	1.12	427 (7.12 min)	No
P3	1,014.81	1,014.68	1.01	18,360 (5.10 h)	No
P4*	1,012.56	–	1.22	66,744 (18.54 h)	No
P5	1,021.83	1,021.49	0.35	0.45	Yes
Constant production rate	1,025.09	–	–	–	–

* The solution to P1 was used as the starting point for P4, see further discussion in text.

respectively. The problems were solved on a 64-bit Windows system with Intel Core i7-2600 CPU at 3.40 GHz and 16 Gb RAM. We note that the first feasible solution to P1 was obtained after 3.26 min CPU time with an optimality gap of 1.09%. Likewise, the first feasible solution to P2 was obtained at 3.73 min with an optimality gap of 4.64%. P1-P3 and P5 used the reference problem (flat production rate at 20 mol/s) as the initial guess for optimization. P4 was started at the MILP solution of P1 to reduce the chance of achieving a locally optimal solution. We note that when P4 was solved starting at the reference problem, the CPU time was 94.62 h with a sub-optimal solution in comparison to P1-P2. Therefore, the following discussion involving P4 refers to the solution reported in Table 4, starting at the optimal solution of P1.

The results indicate that solving P1-P2 results in significant cost savings of 1.12% (when compared to the base case - a scenario where the production rate is kept constant at the value of the demand rate of 20 mol/s). We remind the reader that the electricity prices considered in this study correspond to a period of moderate ambient temperatures (October). It is expected that days with higher ambient temperatures will have higher price variability and the application of this strategy will increase operating cost savings. Also noteworthy, the computation time for P1-P2 is two orders of magnitude lower than in the case of P4 (which uses a full-order model) and 98% lower than P3, where a *nonlinear* SBM is used. The use of LR (P2) lowered CPU time by 4.6 min (0.08 h). In a problem with a higher number of complicating constraints, the reduction in solution time is likely to be more significant.

We also note that, while the optimal value of the objective function for P1 and P2 is the same, there are minor differences in the corresponding setpoint trajectories, suggesting some degree of solution degeneracy for this problem (Fig. 12).

Fig. 11 shows the optimal setpoint sequence calculated by P1 and P2 compared to the optimal sequence obtained using the full-order model in P4, and the optimal sequence based on P5 with rate-of-change constraints. An examination of these trajectories suggests that the maximum rate of change for *decreasing* the setpoint is 4.00 mol/s/h, while the corresponding maximum rate of change for *increasing* the setpoint is 3.52 mol/s/h. This is an indication of the nonlinearity of the system, and also suggests that using a *constant, fixed* rate of change constraint or "ramp rate" (as is often the case, e.g., in optimizing the operation of power systems) could be fraught with two difficulties: if the "ramp rate" is too tight/small, a conservative and economically suboptimal solution is obtained. Conversely, if the ramp rate is too loose/aggressive, the operation of the process is jeopardized, with potential violations in safety and product quality constraints.

Considering the rate-of-change constraint imposed in P5 in light of these observations, we note that while the solution was substantially faster than P1-P4, the chosen maximum step of 0.5 mol/s/h was conservative when applied to all setpoint changes, as evidenced by the predicted cost and actual costs, with savings lower than P1-P4 (0.35%). We emphasize again that multiple attempts at solving P5 were needed to find the ramp-rate constraint (imposed over *all* setpoint changes), which enabled calculation of a dynamically feasible solution when simulated on the full-order process model, resulting in significant effort (which is not reflected in the CPU time of 0.45 s reported for P5).

An additional – and important – observation is that implementing the solution to P5 violates the endpoint constraint PC1, since the holdup in the reboiler at the end of the time horizon was 100 mol lower than the initial holdup amount of 100 kmol. As this (endpoint) constraint is not violated by large setpoint transitions, it is not possible to account for it when optimizing the schedule based on a ramp-rate constraint. In addition, the mismatch between the assumed steady-state behavior in P5 and the actual behavior of the full-order model resulted in a violation of the endpoint storage constraint of 2.0 kmol. This finding further proves the need for embedding dynamics information (in the particular case of rate of change constraint considered here, this would amount to a discretized differential equation capturing the integrating behavior of the reboiler) in the problem formulation for determining a dynamically feasible operating schedule. Plots of the variable trajectories for P1-P5 are given in Fig. 12.

As shown in the figure, the ramp-rate constraint included in P5 leads to a much more gradual change in production rate setpoints. The trajectories of the eight scheduling-relevant variables identified by Pattison et al. [8] are plotted in Fig. 12. Importantly, there are no constraint violations in any of the cases with explicitly embedded dynamics (P1-P4). As such, the remainder of the discussion will focus on the dynamically feasible results from P1-P4, where P1-P2 are the primary focus of this work.

Table 4 shows that the economic benefit is different for P1-P4, with P4 being highest (1.22% cost savings). We assign this discrepancy to the conservative nature of the backoff constraints (particularly in reference to PC1 and QC2) imposed in the solution of P1-P3 to hedge against modeling error. For example, the P4 solution reaches the minimum temperature difference constraint of $1.9°C$ while the P1-P2 solutions are noticeably above this limit. Given that P1-P2 had a backoff constraint of $2.01°C$, it is evident that the reduced-order HW models overestimated $\Delta T_{i,j}$ and therefore the backoff constraint was necessary.

The evolution of the holdup of the storage system is given in Fig. 13. As expected, the storage tank is filled during low electricity demand hours and emptied during peak hours. In addition, the extended time horizon of 72 h allows for storage of extra material for day 2 of the time horizon (Fig. 13), a favorable development given the slightly higher electricity prices on this day (Fig. 2). This is evident in the preemptive increase in storage on day 1, in spite of the fact that day 1 prices are lower in the time period considered (Fig. 2). We remind the reader that this method requires foresight about electricity prices.

The power usage at each time point is given in Fig. 14, where the total energy usage over the 72-h time horizon for P1 is 22.28 MWh. For the case of constant production rate, the total usage is 21.63 MWh. Given that DR requires liquefaction of nitrogen for storage, the DR schemes use slightly more energy than the reference schedule, increasing electricity use by 0.64 MWh (+2.97%). The specific power consumption of our process operating under DR is 0.15 MWh/ton, which is comparable to the overall specific power consumption reported other works, such as [57] for a conventional ASU. We compare the power usage of the ASU with DR and without DR in Fig. 14.

During peak demand times, the optimal DR operating power is below the reference line, showing a reduction in peak power demand. The maximum reduction in peak power demand was by 59.8 MW

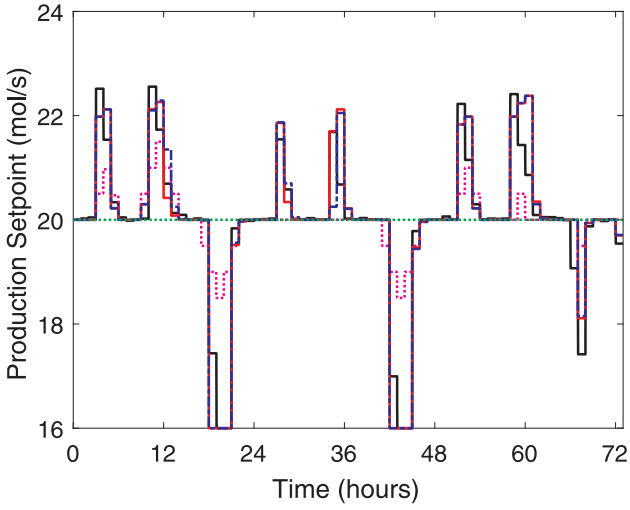

Fig. 11. Plots showing the optimal schedule of setpoints calculated by P1 (red solid), P2 (blue dash-dot), P4 (black dashed), P5 (magenta dotted), and the flat reference (steady-state) line (green dotted). (For interpretation of the references to colour in this figure legend, the reader is referred to the web version of this article.)

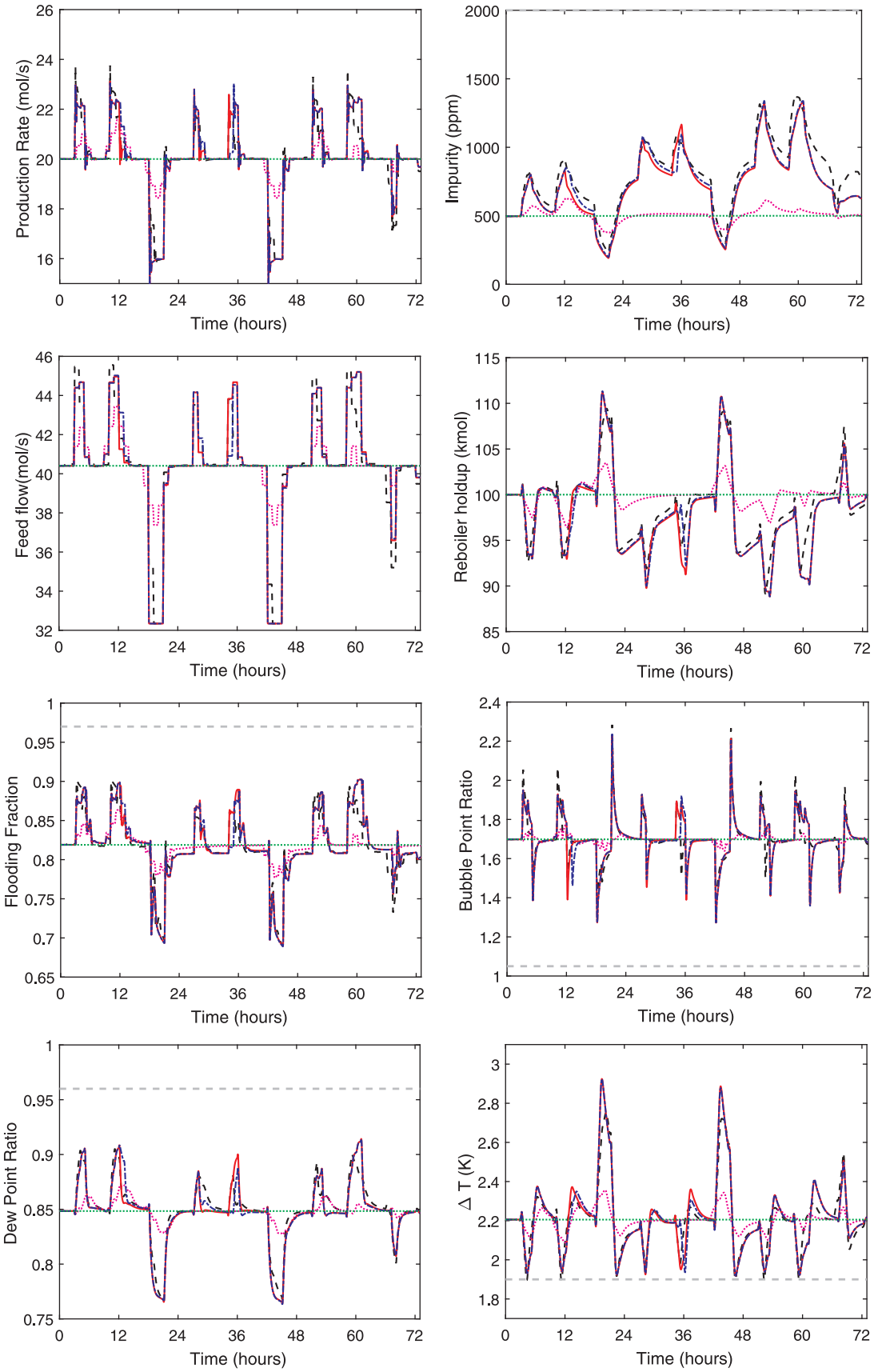

Fig. 12. Plots showing the scheduling-relevant variable trajectories (simulated on the full-order process model) calculated by P1 (red solid), P2 (blue dash-dot), P4 (black dashed), P5 (magenta dotted), and the flat reference (steady-state) line (green dotted). (For interpretation of the references to colour in this figure legend, the reader is referred to the web version of this article.)

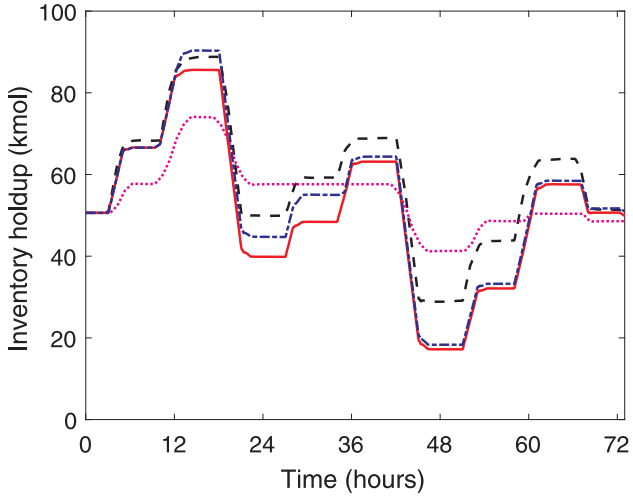

Fig. 13. Storage holdup for P1 (red solid), P2 (blue dash-dot), P4 (black dashed), and P5 (magenta dotted). (For interpretation of the references to colour in this figure legend, the reader is referred to the web version of this article.)

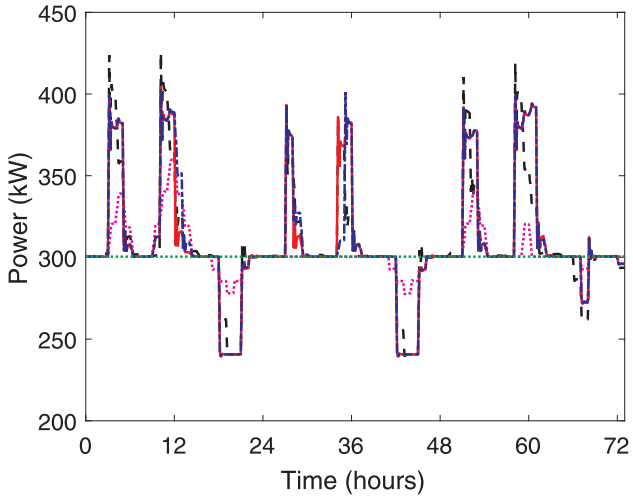

Fig. 14. Time-dependent power usage for P1 (red solid), P2 (blue dash-dot), P4 (black-dashed),P5 (magenta dotted), and the flat reference (steady-state) line (green dotted). (For interpretation of the references to colour in this figure legend, the reader is referred to the web version of this article.)

(−20.0%) for both P1 and P2, which reflects the allowed production setpoint variation of ± 20% of the nominal value (reference problem).

8. Conclusions

In this work, we applied a novel framework for optimal scheduling under dynamic constraints, focusing on an electricity intensive air separation unit (ASU) subject to time-sensitive electricity prices. The chemical plant assists the operation of the grid by providing “demand response” service in response to fluctuations in electricity prices. Specifically, production rates (and power demand) are increased during off-peak hours, when grid load is low and electricity is cheaper. The excess material (in this case, liquid nitrogen) produced is stored, and used to compensate for decreases in production rate, which are imposed during the peak grid demand hours. The central development of this paper is a modeling framework that allows for these highly variable production schedules to be calculated in a very efficient manner (in a matter of minutes for a three-day time horizon), while accounting for the plant dynamics. The latter feature ensures that critical constraints related to the safety of the plant and to the quality of the product are always met. This is the case even as the chemical plant is always operating in a transient regime, as opposed to the more conventional operating paradigm, where a plant would be mostly operated at steady state.

The dynamic plant models that are central to this framework are identified from historical operating data, considerably lowering the effort of model development (compared to the case where a first-principles model is used). Simulations on an industrially-relevant model demonstrated that the proposed modeling strategy is superior to existing approaches of capturing the process dynamics in the form of rate-of-change constraints, which, even when chosen conservatively, can lead to constraint violations during transient operation.

Furthermore, the extensive simulations carried out in this case study showed that the application of this strategy results in considerable cost savings (reducing operating cost by more than 1% in a traditional, well-studied and – at this point – commoditized industry is extremely difficult to achieve). More importantly, ASU DR operation would provide considerable assistance to the operators of the power grid, by dropping the peak grid load presented by the plant by about 20%.

Applying this strategy to all amenable industries could provide grid operators with considerable “breathing room” for incorporating more renewable resources while at the same time reducing the use of hydrocarbon-based power plants, thereby “decarbonizing” the power generation mix. Given that the models used herein are data-driven, we believe this work to be applicable to real situations where historical plant operation data sets are available.

9. Disclaimer

This report was prepared as an account of work sponsored by an agency of the United States Government. Neither the United States Government nor any agency thereof, nor any of their employees, makes any warranty, express or implied, or assumes any legal liability or responsibility for the accuracy, completeness, or usefulness of any information, apparatus, product, or process disclosed, or represents that its use would not infringe privately owned rights. Reference herein to any specific commercial product, process, or service by trade name, trademark, manufacturer, or otherwise does not necessarily constitute or imply its endorsement, recommendation, or favoring by the United States Government or any agency thereof. The views and opinions of authors expressed herein do not necessarily state or reflect those of the United States Government or any agency thereof.

Acknowledgments

This material is based upon work supported by the US Department of Energy under Award Number DE-OE0000841. Partial financial support from the National Science Foundation (NSF) through the CAREER Award 1454433 and Award CBET-1512379 is acknowledged with gratitude.

References

[1] Office of Electricity Delivery and Energy Reliability. Office of electricity delivery and energy reliability; 2017.
[2] Monthly Energy Review. Technical report. US Energy Information Administration; 2017.
[3] US EIA. Manufacturing energy consumption survey; 2013.
[4] ERCOT. Energy reliability council of Texas. URL < http://www.ercot.com/ > ; 2017.
[5] Maravelias CT, Sung C. Integration of production planning and scheduling: overview, challenges and opportunities. Comput Chem Eng 2009;33(12):1919–30. http://dx.doi.org/10.1016/j.compchemeng.2009.06.007. ISSN 00981354.
[6] Grossmann I. Enterprise-wide optimization: a new frontier in process systems engineering. AIChE J 2005;51(7):1846–57. http://dx.doi.org/10.1002/aic.10617. ISSN 0001-1541.
[7] Baldea M, Harjunkoski I. Integrated production scheduling and process control: a systematic review. Comput Chem Eng 2014;71:377–90. http://dx.doi.org/10.1016/j.compchemeng.2014.09.002. ISSN 00981354.

[8] Pattison RC, Touretzky CR, Johansson T, Harjunkoski I, Baldea M. Optimal process operations in fast-changing electricity markets: framework for scheduling with low-order dynamic models and an air separation application. Ind Eng Chem Res 2016;55(16):4562–84. http://dx.doi.org/10.1021/acs.iecr.5b03499. ISSN 0888-5885.

[9] Rush AM, Collins M. A tutorial on dual decomposition and Lagrangian relaxation for inference in natural language processing. J Artif Intell Res 2014;45:305–62. http://dx.doi.org/10.1613/jair.3680. ISSN 10769757.

[10] Paulus M, Borggrefe F. The potential of demand-side management in energy-intensive industries for electricity markets in Germany. Appl Energy 2011;88(2):432–41. http://dx.doi.org/10.1016/j.apenergy.2010.03.017. ISSN 03062619.

[11] Wang X, Tong C, Palazoglu A, El-Farra NH. Energy management for the chlor-alkali process with hybrid renewable energy generation using receding horizon optimization. 53rd IEEE conference on decision and control Los Angeles (CA): IEEE; 2014. p. 4838–43. http://dx.doi.org/10.1109/CDC.2014.7040144. ISBN 978-1-4673-6090-6.

[12] Vinson DR. Air separation control technology. Comput Chem Eng 2006;30(10–12):1436–46. http://dx.doi.org/10.1016/j.compchemeng.2006.05.038. ISSN 00981354.

[13] Emsley J. Nature's building blocks: an A-Z guide to the elements. New York City: Oxford University Press; 2011. ISBN 0199605637.

[14] Manufacturing energy consumption survey: total consumption of electricity. Technical report. Washington (DC): U.S. Energy Information Administration; 2010.

[15] Fu C, Gundersen T. Using exergy analysis to reduce power consumption in air separation units for oxy-combustion processes. Energy 2012;44(1):60–8. http://dx.doi.org/10.1016/j.energy.2012.01.065. ISSN 03605442.

[16] Kansha Y, Kishimoto A, Nakagawa T, Tsutsumi A. A novel cryogenic air separation process based on self-heat recuperation. Sep Purificat Technol 2011;77(3):389–96. http://dx.doi.org/10.1016/j.seppur.2011.01.012. ISSN 13835866.

[17] Fu Q, Kansha Y, Song C, Liu Y, Ishizuka M, Tsutsumi A. A cryogenic air separation process based on self-heat recuperation for oxy-combustion plants. Appl Energy 2016;162(January):1114–21. http://dx.doi.org/10.1016/j.apenergy.2015.03.039. ISSN 03062619.

[18] Miller J, Luyben WL, Blouin S. Economic incentive for intermittent operation of air separation plants with variable power costs. Ind Eng Chem Res 2008;47(4):1132–9. http://dx.doi.org/10.1021/ie070593n. feb ISSN 0888-5885.

[19] Pattison RC, Baldea M. Optimal design of air separation plants with variable electricity pricing. In: Proceedings of the 8th international conference on foundations of computer-aided process design, Washington, DC; 2014. p. 393–8. http://dx.doi.org/10.1016/B978-0-444-63433-7.50050-X.

[20] Cao Y, Swartz CL, Baldea M, Blouin S. Optimization-based assessment of design limitations to air separation plant agility in demand response scenarios. J Process Contr 2015;33(September):37–48. http://dx.doi.org/10.1016/j.jprocont.2015.05.002. ISSN 09591524.

[21] Zhang Q, Grossmann IE, Heuberger CF, Sundaramoorthy A, Pinto JM. Air separation with cryogenic energy storage: optimal scheduling considering electric energy and reserve markets. AIChE J 2015;61(5):1547–58. http://dx.doi.org/10.1002/aic.14730. ISSN 00011541.

[22] Zhang Q, Grossmann IE, Pinto JM. Advances in energy systems engineering; 2017. p. 535–64. http://dx.doi.org/10.1007/978-3-319-42803-1.

[23] Ierapetritou MG, Wu D, Vin J, Sweeney P, Chigirinskiy M. Cost minimization in an energy-intensive plant using mathematical programming approaches. Ind Eng Chem Res 2002;41(21):5262–77. http://dx.doi.org/10.1021/ie011012b. ISSN 0888-5885.

[24] Karwan MH, Keblis MF. Operations planning with real time pricing of a primary input. Comput Oper Res 2007;34(3):848–67. http://dx.doi.org/10.1016/j.cor.2005.05.014. ISSN 03050548.

[25] Mitra S, Grossmann IE, Pinto JM, Arora N. Optimal production planning under time-sensitive electricity prices for continuous power-intensive processes. Comput Chem Eng 2012;38:171–84. http://dx.doi.org/10.1016/j.compchemeng.2011.09.019. ISSN 00981354.

[26] Zhu Y, Legg S, Laird CD. Optimal design of cryogenic air separation columns under uncertainty. Comput Chem Eng 2010;34(9):1377–84. http://dx.doi.org/10.1016/j.compchemeng.2010.02.007. ISSN 00981354.

[27] Adamson R, Hobbs M, Silcock A, Willis MJ. Integrated real-time production scheduling of a multiple cryogenic air separation unit and compressor plant. Comput Chem Eng 2017;104. http://dx.doi.org/10.1016/j.compchemeng.2017.04.001. ISSN 00981354.

[28] Zhou D, Zhou K, Zhu L, Zhao J, Xu Z, Shao Z, et al. Optimal scheduling of multiple sets of air separation units with frequent load-change operation. Sep Purificat Technol 2017;172:178–91. http://dx.doi.org/10.1016/j.seppur.2016.08.009. ISSN 18733794.

[29] Cao Y, Swartz CL, Flores-Cerrillo J. Preemptive dynamic operation of cryogenic air separation units. AIChE J 2017;63(9):3845–59. http://dx.doi.org/10.1002/aic.15753. ISSN 00011541.

[30] Cao Y, Flores-Cerrillo J, Swartz CL. Practical optimization for cost reduction of a liquefier in an industrial air separation plant. Comput Chem Eng 2017;99:13–20. http://dx.doi.org/10.1016/j.compchemeng.2016.12.011. ISSN 00981354.

[31] Du J, Park J, Harjunkoski I, Baldea M. A time scale-bridging approach for integrating production scheduling and process control. Comput Chem Eng 2015;79(August):59–69. http://dx.doi.org/10.1016/j.compchemeng.2015.04.026. ISSN 00981354.

[32] Baldea M, Du J, Park J, Harjunkoski I. Integrated production scheduling and model predictive control of continuous processes. AIChE J 2015;61(12):4179–90. http://dx.doi.org/10.1002/aic.14951.

[33] Baldea M, Daoutidis P. Modeling, dynamics and control of process networks with high energy throughput. Comput Chem Eng 2008;32(9):1964–83. http://dx.doi.org/10.1016/j.compchemeng.2008.02.012. ISSN 00981354.

[34] Jogwar SS, Baldea M, Daoutidis P. Dynamics and control of process networks with large energy recycle. Ind Eng Chem Res 2009;48(13):6087–97. http://dx.doi.org/10.1021/ie801050b. ISSN 0888-5885.

[35] Touretzky CR, Baldea M. Integrating scheduling and control for economic MPC of buildings with energy storage. J Process Contr 2014;24(8):1292–300. http://dx.doi.org/10.1016/j.jprocont.2014.04.015. ISSN 09591524.

[36] Baldea M, Daoutidis P. Dynamics and nonlinear control of integrated process systems. 1st ed. Cambridge (MA): Cambridge University Press; 2012.

[37] Seborg DE, Mellichamp DA, Edgar TF, Doyle FJ. Process dynamics and control. Hoboken (NJ, USA): John Wiley & Sons, Inc.; 2010. http://dx.doi.org/10.1007/s13398-014-0173-7.2. ISBN 9780470128671.

[38] Johansson T. Integrated scheduling and control of air separation unit subject to time-varying electricity price MSc thesis Stockholm (Sweden): KTH Royal Institute of Technology; 2015.

[39] Cao Y, Swartz LE, Christoper, Baldea M. Design for dynamic performance: application to an air separation unit. In: American control conference; 2011. p. 2683–8.

[40] Green DW, Perry RH. Perry's chemical engineers' handbook. 8th ed. New York: Mcgraw-Hill; 2007.

[41] Huang R, Zavala VM, Biegler LT. Advanced step nonlinear model predictive control for air separation units. J Process Contr 2009;19(4):678–85. http://dx.doi.org/10.1016/j.jprocont.2008.07.006. ISSN 09591524.

[42] Harmens A. Vapour-liquid equilibrium N_2ArO_2 for lower argon concentrations. Cryogenics 1970;10(5):406–9. http://dx.doi.org/10.1016/0011-2275(70)90010-X. ISSN 00112275.

[43] Yaws CL, Satyro MA. The yaws handbook of vapor pressure; 2015. ISBN 9780128029992. http://dx.doi.org/10.1016/B978-0-12-802999-2.00001-5. URL < http://www.sciencedirect.com/science/article/pii/B9780128029992000015 > .

[44] Aske EMB, Strand S, Skogestad S. Coordinator MPC for maximizing plant throughput. Comput Chem Eng 2008;32(1–2):195–204. http://dx.doi.org/10.1016/j.compchemeng.2007.05.012. ISSN 00981354.

[45] Narraway LT, Perkins JD. Selection of process control structure based on linear dynamic economics. Ind Eng Chem Res 1993;32(11):2681–92. http://dx.doi.org/10.1021/ie00023a035. ISSN 0888-5885.

[46] Sinnott RK. Chemical engineering design. ELSEVIER – Coulson Richardson's Chem Eng Ser 2005;6(4):440–5.

[47] Billings SA. Nonlinear system identification: NARMAX methods in the time, frequency, and spatio-temporal domains; 2013.

[48] Kelleya Morgan T, Pattison Richard C, Baldick Ross, Baldea Michael. An efficient MILP framework for integrating nonlinear process dynamics and control in optimal production scheduling calculations. Comput Chem Eng 2018;110:35–52. http://dx.doi.org/10.1016/j.compchemeng.2017.11.021. ISSN 00981354.

[49] IBM. CPLEX 12.7; 2017.

[50] GAMS. General algebraic modeling system (GAMS). Release 24.7.4; 2016.

[51] Fisher ML. The Lagrangian relaxation method for solving integer programming problems. Manage Sci 2004;50(12):1861–71. http://dx.doi.org/10.1287/mnsc.1040.0263. ISSN 0025-1909.

[52] Fisher ML. Applications oriented guide to Lagrangian relaxation. Interfaces 1985;15(2):10–21. http://dx.doi.org/10.1287/inte.15.2.10. ISSN 00922102.

[53] Bertsimas D, Tsitsiklis JN. Introduction to linear optimization vol. 30. Hoboken (NJ, USA): John Wiley & Sons, Inc.; 1997. ISBN 1886529191.

[54] Geoffrion AM. Lagrangean relaxation for integer programming. Mathematic programming study 2, vol. 2. Berlin Heidelberg: Springer; 1974. p. 82–114. http://dx.doi.org/10.1007/BFb0120690. ISBN 978-3-642-00739-2.

[55] Bertsekas D. Nonlinear programming. Belmont (MA): Athena Scientific; 1999.

[56] Guignard M. Lagrangean relaxation. Top 2003;11(2):151–200. http://dx.doi.org/10.1007/BF02579036. ISSN 1863-8279 URL <https://doi.org/10.1007/BF02579036>.

[57] Aneke M, Wang M. Potential for improving the energy efficiency of cryogenic air separation unit (ASU) using binary heat recovery cycles. Appl Therm Eng 2015;81:223–31. http://dx.doi.org/10.1016/j.applthermaleng.2015.02.034.